Flow Dichroism as a Reliable Method to Measure the Hydrodynamic Aspect Ratio of Gold Nanoparticles

Naveen Krishna Reddy,[†] Jan Vermant,[*,†] Jorge Perez-Juste,[‡] Isabel P. Santos,[‡] Luis M. Liz-Marzan,[‡] Peter R. Lang,[¶] and Jan K. G. Dhont[¶]

Department of Chemical Engineering, K.U. Leuven, W. de Croylaan 46, B-3001 Leuven, Belgium, Departamento de Quimica Fisica and Unidad Asociada CSIC, Universidade de Vigo, 36310, Vigo, Spain, and Institute for Festkorperforschung Forschungszentrum, Juelich, D-52425 Juelich, Germany

E-mail: jan.vermant@cit.kuleuven.be

Phone: + 32 16 32 23 55. Fax: + 32 16 32 29 91

Abstract

Particle shape plays an important role in controlling the optical, magnetic and mechanical properties of nanoparticle suspensions as well as nanocomposites. However, characterizing the size, shape and the associated polydispersity of nanoparticles is not straightforward. Electron microscopy provides an accurate measurement of the geometric properties, but sample preparation can be laborious and to obtain statistically relevant data many particles need to be analyzed. More importantly practical applications are not always governed by the geometric properties but rather by hydrodynamic properties. Methods that evaluate the dynamics of nanoparticles such as light scattering and rheo-optical methods accurately provide hydrodynamic properties, but do necessitate a sufficient optical response. In the present work, different

[*]To whom correspondence should be addressed
[†]K.U. Leuven
[‡]Universidade de Vigo
[¶]Institute for Festkorperforschung Forschungszentrum

methods for characterizing non-spherical gold nanoparticles are critically compared, especially taking into account the complex optical response of these particles. The different methods are evaluated in terms of their versatility to asses size, shape and the polydispersity. Among these, the rheo-optical technique is shown to be the most reliable method to obtain hydrodynamic aspect ratio and polydispersity for non-spherical gold nanoparticles for two reasons. First, the use of the evolution of the orientation angle makes effects of polydispersity less important. Second, the use of an external flow field gives a mathematically more robust relation between particle motion and aspect ratio.

Introduction

Non-spherical nanoparticles are being extensively used as basic building blocks to construct large scale structures having controlled shapes and sizes, with tailored chemical and mechanical properties, all the way to design devices with unique optical and electrical properties[1] . Promising novel applications of nano sized non-spherical particles include those that use the localized surface enhanced Raman effect[2] , exploit the single electron tunneling[2] or focus on high strength and conductivity in nanocomposite polymers[3] . Other applications use the nanoparticles as fluorescence enhancers[4] , as a source for strong local heating[5] , as waveguides for sub-wavelength photonics integration[7] or finally for their use in high density recording media[8] . Another important reason for studying non-spherical particles is that the colloidal domain is dominated by non-spherical particles, where 90% of particles found in nature are disks, 9% are rods and the remaining 1% includes all the other shapes. However, most research so far has focused on spherical colloids and micro particles. Even biological particulate systems are dominated by anisotropic shapes, like red blood cells which are oblate or rod-like actin and microtubules which are used for strengthening the cells cytoskeleton[9,10] . In the majority of applications, either during the production process or in the final product, nanoparticles are suspended in a fluid. A knowledge of hydrodynamic dimension and the associated polydispersity are essential in understanding the effect of non-spherical nanoparticles on phenomena such as self assembly[11] and directed self-assembly[12] and the dynamics of

phase transition[13] .

Electron microscopy (EM) is used extensively to determine dimensions of non-spherical nanoparticles. The characterization of nanoparticles by electron microscopy is based on generating an image of the particles by collecting secondary or backscattered electrons in the case of scanning electron microscopy (SEM) and from transmitted electrons in the case of transmission electron microscopy (TEM)[15] . For TEM a drop of suspension containing nanoparticles is dried on a grid before imaging. Due to small sample volume, tens of EM images have to be processed to get a reasonable statistics on the nanoparticle dimensions. This process is time consuming, expensive and most often only a limited number of particles is counted, and the statistics are typically poor. The size obtained from electron microscopy gives a physical dimension of the particle in the dried state and does not necessarily represent the nanoparticles in suspension, where for example the electroviscous-effects, adsorbed polymer, surfactant or hydration layers change the effective hydrodynamic dimensions[16] .

The present work compares methods to analyze the hydrodynamic properties of non-spherical gold nanoparticles. More specifically, we focus on depolarized dynamic light scattering (DDLS) and flow induced dichroism. Although the elastic scattering for nanoparticles particles is weak, non-spherical gold nanoparticles exhibit an anisotropy in polarizability due to the surface plasmon effect[5,6] . The surface plasmon arises due to transverse and longitudinal electron oscillations which lead to both scattering and absorption. The presence of surface plasmons causes the polarization of the scattered light to depend on the orientation of the particles[6] . This dependence on orientation can be exploited in DDLS to obtain the translational (D_t) and the rotational (D_r) diffusion coefficients, by measuring time-auto correlation functions of the scattered light with polarization parallel and perpendicular to the incident beam polarization. The two diffusion coefficients are related to hydrodynamic dimensions (length and width), although for short particles the effect of finite length is not trivial to account for.

DDLS investigates the fluctuations in orientation and position due to Brownian motion in a randomly oriented suspension. The optical responses from an oriented suspension will be different. In rheo-optical measurements, the transient optical response of a suspension subjected to flow is used to measure the particle properties. For example, it has been shown that the time evolution of the polarized UV-vis absorption can be used to obtain a hydrodynamic dimension[14] . Here we use an even more simple polarimetric method to measure the time evolution of the anisotropy in the refractive index tensor. A well defined flow field is applied in order to control the motion of the particles[17] . Non-spherical particles in flow tumble due to a difference in torque between the two ends of the particle provided that the local velocity gradients are high enough, such that the motion is determined solely by the hydrodynamics forces. Provided that the convective force overwhelms the force associated with the Brownian motion (as characterized by the Péclet number), when the flow is started up the time dependent optical response of the particles will show a damped oscillatory behavior due to the effect of the tumbling motion of the particles on the overall orientation distribution function (ODF). The tumbling period of the ODF depends on the hydrodynamic aspect ratio of the particles. Differences in tumbling periods of the individual particles due to different particle aspect ratio lead to phase mixing, which dampens the optical response of the integrated ODF in time to a steady state value. The associated polydispersity in aspect ratio of nanoparticles can be extracted by analyzing the decay of optical response of the ODF due to phase mixing. The challenges for using this method for nanoparticles are a) sufficient scattering intensity and b) sufficiently high Péclet number.

Both gold nanorods (Au-nanorod) and decahedral gold nanoparticles (Au-deca) will be studied. The gold nanorods were suspended in an aqueous matrix and stabilized by the surfactant Cetyl trimethylammonium bromide (CTAB). The decahedral gold nanoparticles obviously have the same shape, but their size differs. These Au-deca particles are stabilized by a layer of Polyvinylpyrrolidone (PVP). The details of gold nanoparticles synthesis is given in the materials section at the end

of this article. For DDLS experiments, the gold nanoparticles are dispersed in water so that the Brownian motion of the nanoparticles can be easily detected. On the other hand, for rheo-optical measurements the gold nanoparticles are dispersed in 99.5% glycerol to increase the medium viscosity and to bring the high Péclet number regime into experimental range. The particles will be characterized by electron microscopy, DDLS studying Brownian dynamics and finally by rheo-optical method investigating flow field enforced dynamics. We evaluate the sample preparation procedures, measurements errors and the relevance of the above three methods for both rod-like and disk shaped decahedral gold nanoparticles. By comparing the three methods, we show that, the flow dichroism is the most reliable method to determine hydrodynamic aspect ratio of non-spherical nanoparticles.

Results

Electron microscopy

For all non-spherical nanoparticles electron microscopy is a suitable method to obtain physical dimensions and the associated polydispersity using quantitative image analysis. For TEM, a drop of nanoparticle suspension is placed on a TEM grid and then allowed to dry before placing the grid inside the TEM. Images of the nanoparticles are taken by adjusting the electron beam energy, to get optimum contrast. Typical micrographs obtained from electron microscopy of rod-like (Au-nanorod-2) and disk-like (Au-deca-3) are shown in Figure 1.A and B. The corresponding geometric dimensions of nanoparticles obtained from image analysis using the UTHSCSA ImageTool software[18] are listed in table 1, and are an average over 150-200 particles. For Au-decas only the length of one edge can be measured from the TEM images. Since the Au-decas are decahedral in shape, their aspect ratio should satisfy the golden ratio rule $(1+\sqrt{5})/2$. In table 1, diameter for Au-decas are calculated from this golden ratio.

The standard error on the arithmetic mean of the geometric aspect ratio (AR) of gold particles with a standard deviation (ρ) is given as $\rho/\sqrt{n}$, where n is the number of particles analyzed to

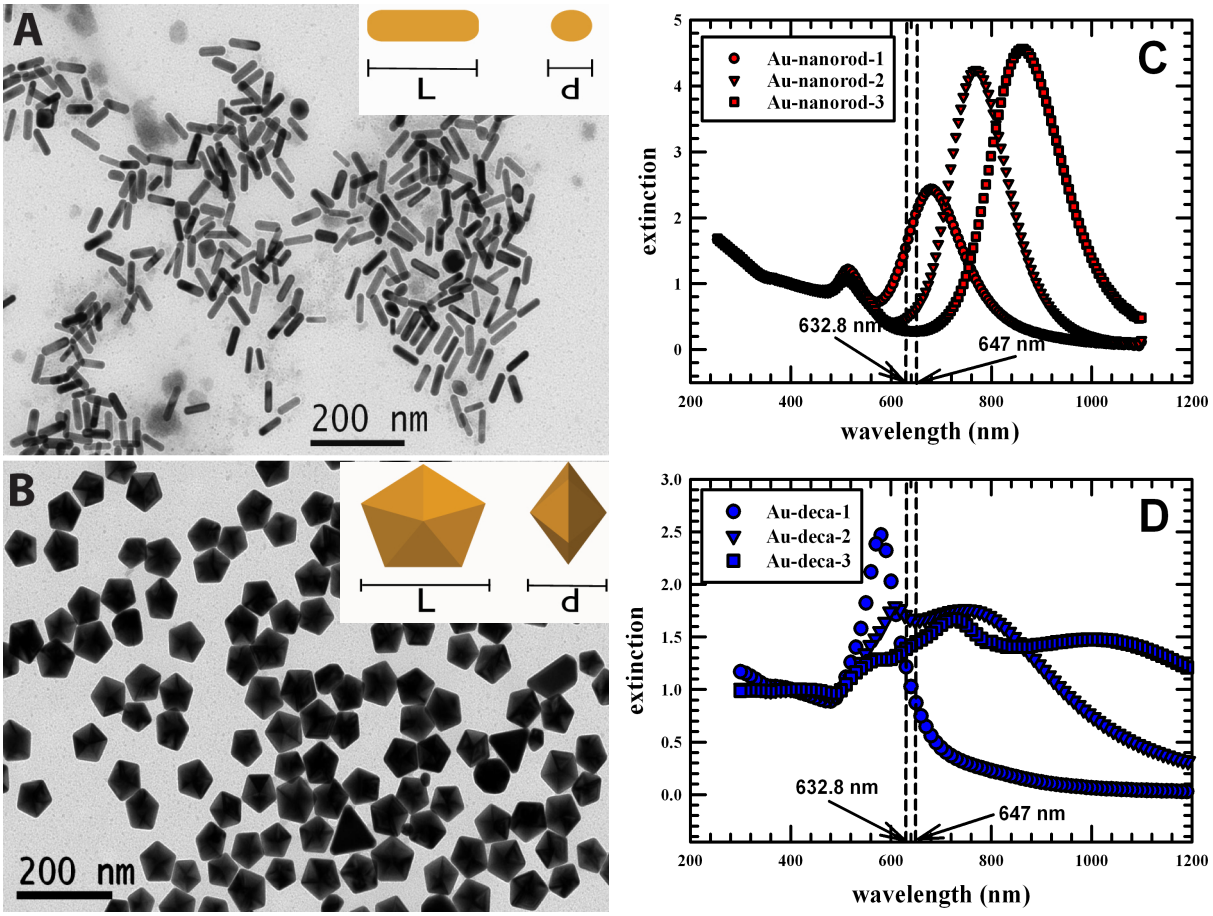

Figure 1: Transmission electron micrographs and extinction spectra of non-spherical gold nanoparticles. A) Au-nanorod-2 and B) Au-deca-2 (JEOL 1010, 100 kV Scale bar = 200 nm.) C) Extinction spectra for Au-nanorods D) Extinction spectra for Au-nanodecas. Insect in A) and B) are illustrations showing the measured dimensions, listed in Table 1.

Table 1: Average geometric nanoparticle dimensions (L,d), geometric aspect ratio (AR) measured from TEM and estimated hydrodynamic aspect ratio (P_{TEM}).

Sample	L (nm)	d (nm)	AR	P_{TEM}
Au-nanorod-1	56.0 ± 6.0	20.0 ± 3.0	2.70 ± 0.50	2.3
Au-nanorod-2	61.0 ± 7.0	18.0 ± 0.5	3.40 ± 0.50	2.8
Au-nanorod-3	66.0 ± 6.0	15.0 ± 2.0	4.30 ± 0.60	3.4
Au-deca-1	43.0 ± 2.0	26.0 ± 1.2	0.62 ± 0.03	0.62
Au-deca-2	100.0 ± 6.0	62.0 ± 3.7	0.62 ± 0.025	0.63
Au-deca-3	172.0 ± 5.0	105.0 ± 2.5	0.62 ± 0.015	0.61

obtain the mean and the ρ. To have a standard error of 1%, 10^4 particles have to be analyzed. For our case we measured 150-200 particles (approximately the number of particles in an image) and to get to 1% standard error we need to analyze 50-60 images, which is time consuming. Moreover, the main drawback with this method is that it does not provide direct information about hydrodynamic aspect ratio. It has been proposed that the hydrodynamic aspect ratios can be calculated by adding the estimated thickness of the stabilizing layer to the geometric dimensions obtained from TEM. This empirical method provides an estimate for the hydrodynamic aspect ratio, referred to as P_{TEM}. The stabilizing layer for Au-nanorods is Cetyl trimethylammonium bromide (CTAB) of length 3.2 nm, and it is assumed to be present on all the sides of the nanorod[29,30] . For Au-decas the stabilizing layer is made of polyvinylpyrrolidone (PVP) with a molecular weight of 40,000 Da, which has a thickness of 2 nm[31] .

The particle sizes and shapes are such that the particles will posses an anisotropic optical response, not only because of the mere geometric properties, but mainly because of the presence of the surface plasmon[32,33] . The extinction curves as a function of wavelength are given in Figure 1.C for the Au-nanorods. As the aspect ratio of the rods is decreased, the plasmon resonance peak shifts to smaller wavelengths and the peak decreases in intensity. However, at the wavelengths used in the light scattering and rheo-optical experiments, the particles with the smallest aspect ratio show the strongest extinction. As the width of the rods is smaller than 30 nm, most of the extinction will come from absorption[33] . For the decahedral gold disks, the extinction curves in Figure 1.D are less clear but for all particles there is sufficient extinction to provide contrast at the wavelengths used in the optical setups.

Depolarized dynamic light scattering

Dynamic light scattering is a standard technique in particle sizing and is typically based on the elastic scattering of light by particles undergoing Brownian motion in a suspension. The time correlation of the intensity fluctuations is a direct measure of the Brownian motion of the particles[19]

. For an ensemble of monodisperse particles, the field correlation function is an exponentially decaying function $g_1(q,t) = \exp\{-\Gamma t\}$, where Γ is the relaxation rate, q is the scattering vector and t is the correlation time. Γ is related to the particles' translational diffusion. The translational diffusion coefficient (D_t) is related to the particles' effective hydrodynamic radius by the Stokes-Einstein-Sutherland equation[20,21] .

If the particles exhibit sufficiently large shape or optical anisotropy or both, orientational terms will contribute to the relaxation rate.[23,24] This in principle allows the determination of the rotational diffusion coefficient D_r provided the state of polarization of the scattered light is considered in the data analysis. Here, we use depolarized dynamic light scattering technique to determine both translational and rotational diffusion coefficients for gold nanorods. The analysis of DDLS method for obtaining D_t and D_r for gold nanorods similar to the one used in this work are described in detail by Rodriguez-Fernandez et al.[22] . Briefly, the intensity auto correlation functions obtained from light scattered in the so-called vertical-vertical (VV) and vertical-horizontal (VH) modes are fitted by using Eq. (1) and Eq. (2)[22] ,

$$g_2^{VV}(q,t) - 1 = \beta[A^2 \exp\{\{-\Gamma_2 t\}\} + 2AB\exp\{\{-(\Gamma_2 + \Delta/2)t\}\} + B^2 \exp\{\{-(\Gamma_2 + \Delta)t\}\}] \quad (1)$$

$$g_2^{VH}(q,t) - 1 = \beta' \exp\{\{-(\Gamma_2 + \Delta)t\}\} \quad (2)$$

Here $\Gamma_2 = 2\Gamma = 2D_t q^2$ and $\Delta = 12D_r$, while $A + B = 1$ are related to the anisotropy of the particles' polarizability. The parameters β and β' account for the non-ideality in the light scattering setup and are smaller than unity[22] . A non-linear least square fitting global algorithm based on an evolution algorithm is used to determine the parameters which fit best eqs.Eq. (1) and Eq. (2) to the experimental data of 19 VH and VV correlation functions respectively, spanning from 40 ^{o}-130^o. In this procedure A, D_t, and D_r are treated as global parameters, while β and β' are allowed to vary between different correlation functions. Examples of the experimentally measured

correlation functions are shown in Figure 2, for Au-nanorod-1 in VV and VH mode. For clarity, the auto correlation function are plotted for angles of 40^o, 60^o, 120^o only. Lines in Figure 2 are non-linear least-square fits to eqs.Eq. (1) and Eq. (2).

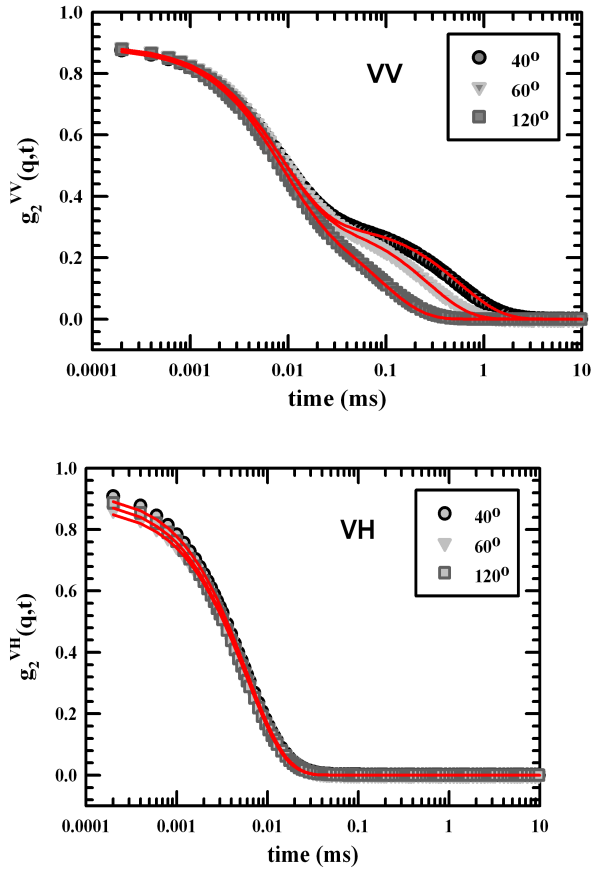

Figure 2: Typical auto correlation functions for Au-nanorod-1 suspensions recorded in VV and VH modes at 40, 60, 120^o. The lines are fits to eq. 1 and 2.

To derive the hydrodynamic aspect ratio from the experimental data, a relationship between the diffusion coefficients and the hydrodynamic dimension is required. For infinitely thin rods of length (L) and aspect ratio (P_{DDLS}) in a fluid of viscosity (η) and temperature (T) slender body results of Boersma and Brenner are available[26,27] . For small aspect ratios correction factors C_t and C_r are required to account for the relative importance of end effects due to the finite rod length[28] . The modified Brenner equations can be combined to yield an implicit relation between the aspect

ratio and the diffusivities:

$$f(P_{DDLS}) = \left\{ \frac{9\pi\eta}{k_B T} \right\}^{2/3} \frac{D_t}{D_r^{1/3}} = \frac{ln(P_{DDLS}) + C_t}{(ln(P_{DDLS}) + C_r)^{1/3}} \tag{3}$$

where,

$$C_t = 0.312 + 0.565 P_{DDLS}^{-1} - 0.100 P_{DDLS}^{-2} \tag{4}$$

$$C_r = -0.662 + 0.917 P_{DDLS}^{-1} - 0.050 P_{DDLS}^{-2} \tag{5}$$

The numerical value obtained for $f(P_{DDLS})$ by substituting a value for P_{DDLS} into the right hand side of equation 7 must equal to numerical value of $f(P_{DDLS})$ obtained by substituting D_t and D_r both obtained experimentally.

Table 2: Mean translational diffusion (D_t), mean rotational diffusion (D_r) from DDLS and the corresponding hydrodynamic aspect ratio calculated from equation Eq. (3). For comparison hydrodynamic aspect ratio calculated by adding stabilizing layer thickness to the TEM data is also shown (P_{TEM}).

Sample	D_t (1E4) (nm^2/ms)	D_r (1/ms)	P_{DDLS}	P_{TEM}
Au-nanorod-1	1.09 ± 0.06	15.1 ± 0.1	1.85 ± 0.65	2.3
Au-nanorod-2	0.99 ± 0.04	15.3 ± 0.2	1.35 ± 0.47	2.8
Au-nanorod-3	0.96 ± 0.02	12.2 ± 0.3	1.55 ± 0.54	3.4

D_t and D_r were obtained from the correlation functions using the global fits for the three gold rods and are give in Table 2. The relation between D_t and D_r and P_{DDLS}, given by equation Eq. (3), is represented graphically in Figure 3 along with the hydrodynamic aspect ratio calculated using equation Eq. (3), given as P_{DDLS}. The calculated hydrodynamic aspect ratio for Au-nanorod-1 as obtained using DDLS agree with the earlier provided estimate for P_{TEM}. The expected increase of hydrodynamic aspect ratio for Au-nanorod-2 and 3 is not recovered by the DDLS analysis. For these particles, the measurements in Figure 1.C showed that surface plasmon leads to only a small

extinction at the wavelength used in the light scattering (647 nm). The scattering by the surface plasmon due to the small extinction will be weaker, leading to a worsened signal to noise ratio. Additionally, DDLS analysis does not take polydispersity into account, thus hydrodynamic aspect ratio obtained from DDLS shows large deviations from P_{TEM}.

In this respect it should be noted that P_{DDLS} is inside the logarithm in equation Eq. (3). A simplified sensitivity analysis can be used to estimate the effect of small variations in D_t and D_r on the calculated hydrodynamic aspect ratio. A detailed 3D plot of P_{DDLS} as a function of D_t and D_r, in Figure 3, shows that an error in D_t, has a larger effect on aspect ratio of the particles as compared to an error in D_r. A 5% error in obtaining both D_t and D_r, a typical value for dynamic light scattering measurements, which includes experimental errors and errors in curve fitting, translates to 30-40% error in calculated aspect ratio, lines in Figure 3. This large error is due to the fact that P_{DDLS} is inside the logarithm in equation Eq. (3). Finally, the samples are somewhat polydisperse and it is hard to asses the effect of shape and size polydispersity in presence of the surface plasmons. Purely elastic scattering will be dominated by the larger particles, for the surface plasmon there is a more complex dependency on particle size and shape[33] .

The analysis of the DDLS data for Au-decas is even more complex due to the different polarization directions of the scattered light by the decahedron shaped particles, especially in the presence of the surface plasmon. The expressions for normalized intensity autocorrelation functions for disks of complex shapes is not yet available. This disadvantage of DDLS, as with any method that employs scattering, the relationship between the scattering intensity and the correlation function needs to be known a priori for the particles with different shapes and polydispersity, which are not known before hand.

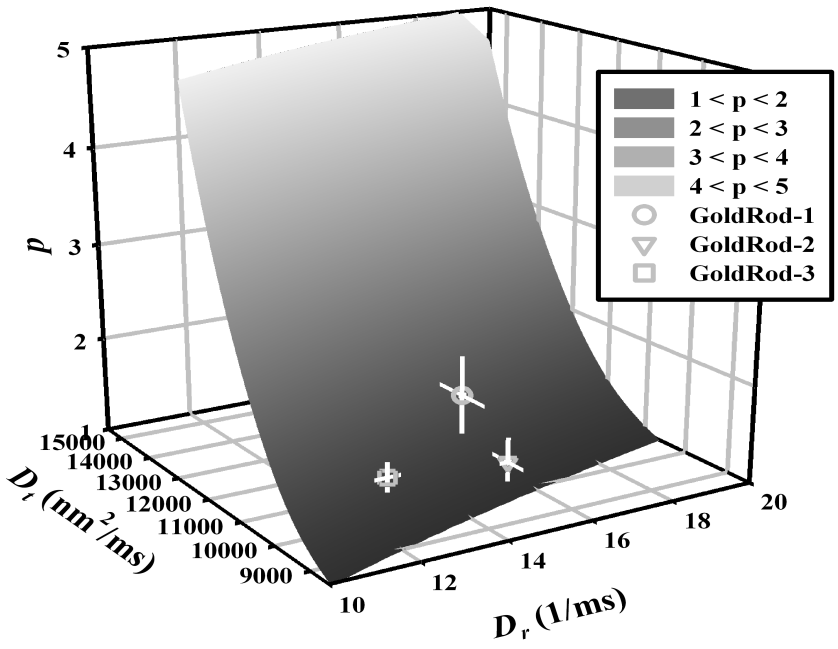

Figure 3: 3D plot of aspect ratio (P_{DDLS}) as a function of translational diffusion (D_t) and rotational diffusion (D_r) following equation Eq. (3). The symbols are experimentally determined values of D_t and D_r and the corresponding P_{DDLS}. The crosses are errors in measuring D_t, D_r and the corresponding error in calculating P_{DDLS}.

Rheo-optical measurements

To circumvent some of the inherent limitations of the DDLS, the use of rheo-optical measurements is explored. First, a well defined flow field is used which determines the particle motion and leads to a simpler relation between aspect ratio and the observed optical response as will be discussed below. Second, the measured dichroism will be determined by both the scattering and absorption of the particles, hence leading to a more pronounced optical response for the gold nanoparticles. The quantitative calculation of dichroism for these small gold particles is even more difficult compared to the scattering properties and using dichroism to back calculate for example polydispersity effects is not trivial. However, as the surface plasmon is determined by the aspect ratio of the anisotropically shaped particles, the evolution of average orientational angle of the particles can be used. The orientation angle is not dependent on scattering theory and the associated complicated effects of

polydispersity unlike the scattering or absorption properties, and hence its magnitude does not directly depend on the size of the particles. Following earlier work for scattering dichroism[36,40] , the time evolution of the orientation distribution function (ODF) can be used to determine the aspect ratio of the particles. For monodisperse rods, the orientation distribution function upon inception of flow at high Péclet numbers will be an oscillatory function in time. As a consequence the optical properties such as the dichroism will oscillate in time. When polydispersity of the hydrodynamic aspect ratio, stemming from both size and shape, is present, the oscillatory behavior of the ODF upon start-up of flow will be damped due to phase mixing[36] . The decay of orientation angle to a constant value due to phase mixing is a quantitative measure of the degree of polydispersity, higher polydispersity resulting in a faster decay.

Starting with the motion of a single particle, the time evolution of the ODF and the average orientation angle can be developed. The creeping flow equations for spheroidal particles in a Newtonian fluid subjected to simple shear flow was solved by Jeffery[34] . The forces acting on spheroid can be reduced to two torques, due to which particles tumble in flow. In a simple shear flow the evolution equation of the orientation of the major axis of an individual, non-Brownian, neutrally buoyant spheroid with aspect ratio P_D describes a motion given by,

$$\tan\theta = \frac{C.P_D}{(P_D^2\cos^2\phi + \sin^2\phi)^{0.5}} \tag{6}$$

$$\tan\phi = P_D \tan\left\{\frac{2\pi t}{T} + \kappa\right\} \tag{7}$$

where θ and ϕ are the first and second Euler angles. C and κ are constants of integration determined by the initial conditions. T is the period of rotation determined by the particle aspect ratio (P_D, as measured using dichroism) and shear rate ($\dot{\gamma}$).

$$T = \frac{2\pi}{\dot{\gamma}}\left\{P_D + \frac{1}{P_D}\right\} \tag{8}$$

For the motion of any rigid axis-symmetric body, Breherton[39] obtained a similar equation as Jeffery (Eq. (8)) were P_D was the equivalent hydrodynamic aspect ratio. It has to be noted that the aspect ratios for Au-decas are calculated assuming that they are oblate ellipsoids. Since Au-deca has well defined faces, the true volume of an Au-deca will be smaller than that calculated by treating it as an oblate ellipsoid.

The hydrodynamic aspect ratio has been determined from experimental measurements of either turbidity[35] , scattering dichroism[36–38] or UV-Vis absorption[14] . In the present case of the gold particles the dichroism arises from both scattering and intrinsic dichroism contributions, but these are assumed to be coaxial. Dichroism and orientation angle are simultaneously calculated from the harmonic coefficients (see methods section). The extinction coefficient δ'' is given in the monograph of Fuller as[17]

$$\delta'' = -sgn(R_2)tanh^{-1}\left\{\frac{1}{2}\sqrt{\frac{R_1}{-J_1(A)}+\frac{R_2}{-J_2(A)}}\right\} \tag{9}$$

where J_1(A) and J_2(A) are Bessel functions of the zeroth kind. The dichroism is related to the extinction coefficient by:

$$\Delta n'' = \frac{\delta''\lambda}{2\pi l} \tag{10}$$

where l is the optical path length and λ is the wavelength of the light source. The magnitude of dichroism is related to the average orientation of the particles induced by flow. In the steady state, the average dichroism and orientation angle of all the particles is constant, and on average the particles spend more time along the flow direction. To obtain polydispersity it is necessary to measure the phase mixing in the ODF that occurs under transient flow conditions.

To obtain the hydrodynamic aspect ratio and the associated polydisperisty, a non linear fit to the time dependent average ODF is used as developed by Vermant et al.[40] . For small aspect ratio particles an expression for orientation angle as a function of aspect ratio and polydisperisty is given by:

$$tan2\chi = \frac{2\int_0^\infty (P_D - P_D^{-1}) sin\frac{4\pi t}{T} g(P_D) dP_D}{\int_0^\infty \left\{ P_D^2 - P_D^{-2} - (P_D^2 - P_D^{-2}) cos\frac{4\pi t}{T} \right\} g(P_D) dP_D} \tag{11}$$

where $g(P_D)$ is an assumed to be a Gaussian distribution function of the hydrodynamic aspect ratio

$$g(P_D) = \frac{1}{\sqrt{2\pi\sigma^2}} exp\left\{ \frac{-(P_D - \bar{P_D})^2}{2\sigma_D^2} \right\} \tag{12}$$

and T is the period of rotation, given by Eq. (8). Using Eq. (11), the average hydrodynamic aspect ratio ($\bar{P_D}$) and the corresponding polydispersity (σ_D) are determined.

The set of equations describing the transient flow are only valid in the flow regime were rotational Brownian motion is dominated by the convective forces, i.e. the high Péclet number regime. In order to determine this regime the steady state properties need to be measured first. As an example of typical experimental results of the evolution of the steady state dichroism and the average orientation angle, results are given for a suspension of Au-deca-2 in Figure 4. At low shear rates, due to the dominance of rotational Brownian motion the distribution of orientations remains close to isotropic, the magnitude of dichroism is small and the average orientation angle is still large. When the shear rate is increased the hydrodynamic forces become dominant and tumbling particles spend most of their orbit in an orientation close to the flow direction. On average, the orientation of the particles long axis is close to the flow direction and the magnitude of dichroism increases as in Figure 4. The critical shear rate at which the hydrodynamic forces become dominant is taken as the lower limit for the transient experiments.

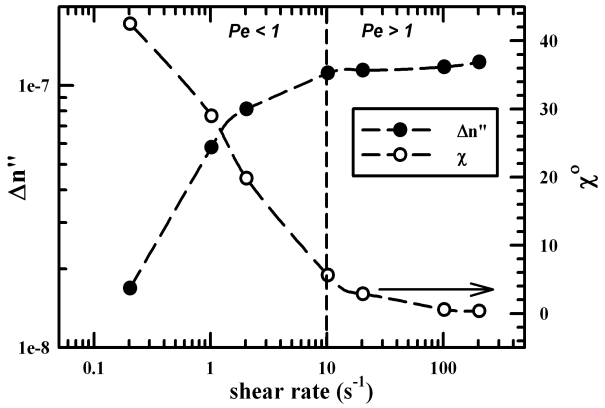

Figure 4: Dichroism and orientation angle as a function of shear rate for Au-deca-2 in 99.5 % glycerol

In the transient experiments, flow is started above the critical shear rate for a suspension which has been rendered isotropic by the effects of Brownian motion. When flow is started in the high Péclet regime, the tumbling of the particles causes the transient response to show an oscillatory response of the dichroism (data not shown) and orientational angle, shown in Figure 5 (Au-nanorods) and Figure 6 (Au-decas). The oscillatory response is damped because particles with different aspect ratios have different tumbling periods, and hence phase mixing occurs. The signal to noise ratio for the Au-decas is good, due to the high extinction value of light at 632.8 nm due to presence of the surface plasmon (Figure 1.D). Similar results are obtained for the Au-nanorods, Figure 1.C, but the S/N ratio is less good. For Au-nanorod-2 due to the low extinction value the measured transient signal had large amount of noise associated with the signal (Figure 5).B. Finally, for the long aspect ratio Au-nanorod-3, the light extinction values at 632.8 nm is extremely low and the diameter is small, due to which we could not measure reliable signal. Table 4 shows a list of hydrodynamic aspect ratio measured through dichroism and the corresponding polydispersity obtained by non-linear fit of Eq. (11) to the transient data.

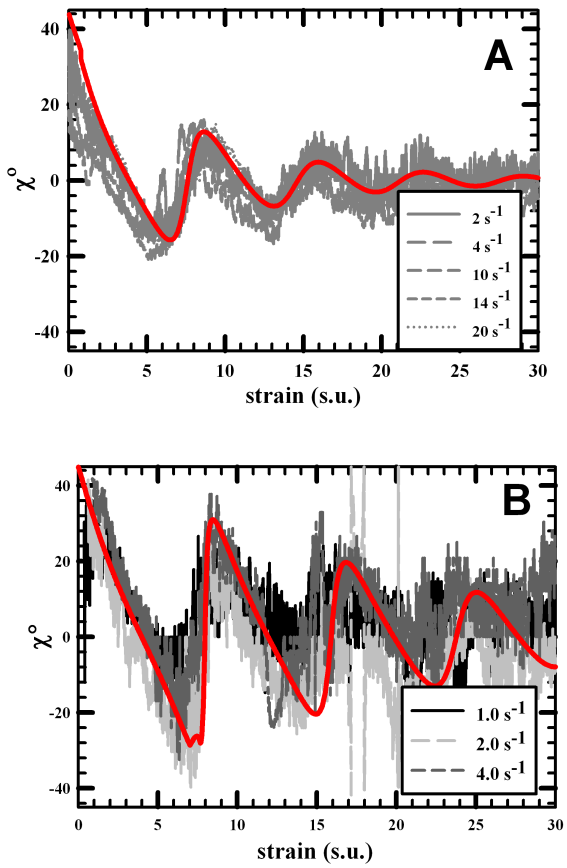

Figure 5: Orientation angle as a function of strain for A) Au-nanorod-1 and B) Au-nanorod-2.

Table 3: Hydrodynamic aspect ratio and the corresponding polydispersity of gold nanoparticles obtained from flow startup dichroism experiments.

Sample	P_D	σ_D
Au-nanorod-1	1.7 ± 0.1	0.14 ± 0.03
Au-nanorod-2	2.0 ± 0.1	0.05 ± 0.02
Au-deca-1	0.47 ± 0.03	0.17 ± 0.04
Au-deca-2	0.55 ± 0.02	0.16 ± 0.03
Au-deca-3	0.55 ± 0.01	0.05 ± 0.01

Discussion

Aspect ratios obtained from TEM, DDLS and dichroism are compared in table 4. The hydrodynamic aspect ratios obtained from DDLS using Eq. (3) (P_{DDLS}) does not always provide accurate

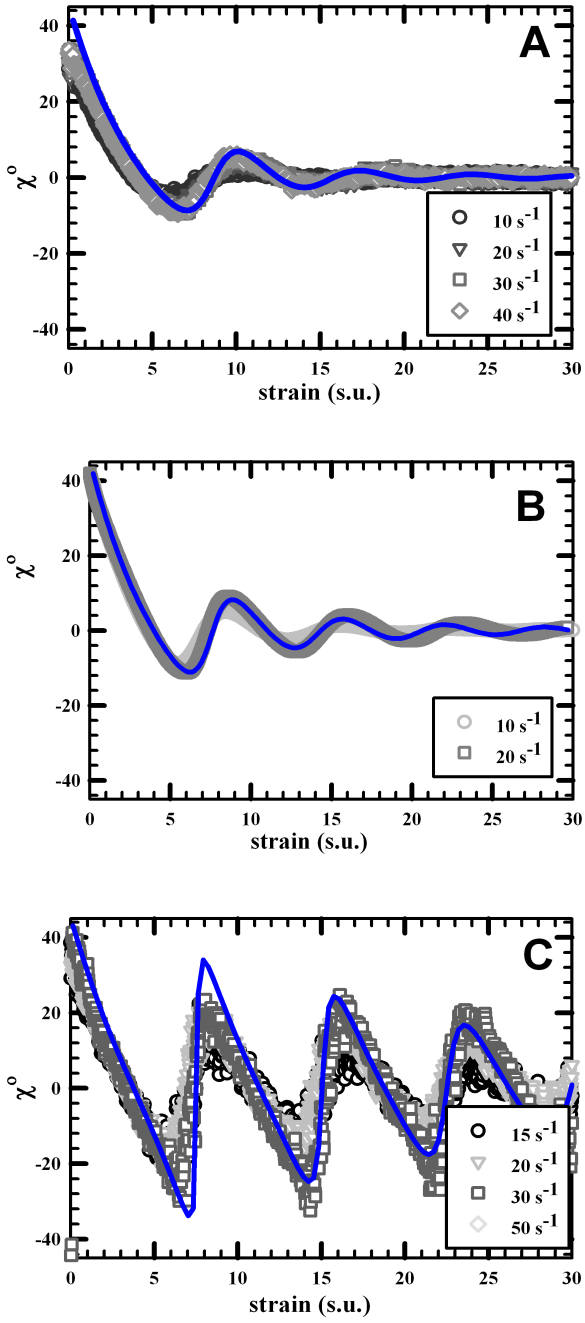

Figure 6: Orientation angle as a function of strain for A) Au-deca-1, B) Au-deca-2 and C) Au-deca-3.

results except for Au-nanorod-1. Many authors have used DDLS to measure hydrodynamic aspect ratio and have found large differences between microscopy techniques and DDLS. For instance, Rodriguez-Fernandez et al.[22] measured the hydrodynamic aspect ratio of gold rods that qualitatively agree well with the calculated P_{TEM}. If however, hydrodynamic aspect ratio is computed from Eq. (3) using their data, we see that values of P_{DDLS} are almost 50% smaller than those estimated from P_{TEM} estimated by adding CTAB layer thickness[22] . Similarly, hydrodynamic aspect ratios for single walled carbon nanotubes calculated from DDLS measurements gave almost an order of magnitude differences when compared with AFM results[25] . The main reason behind the large errors in obtaining the hydrodynamic aspect ratio using DDLS seems to be the high sensitivity of diffusion coefficients to aspect ratio. Invariably the aspect ratio is inside the logarithmic function which magnify the errors in solving the inverse problem.

The hydrodynamic aspect ratios obtained from rheo-optics is in better agreement with the estimated value and trends from TEM measurements. The main reason for this is the fact that dichroism is based on the optical response of the nanoparticles in flow. In the case of dichroism the nanoparticles are suspended in a high viscous fluid where they move only when flow is applied due to which a controlled optical response can be measured accurately and the relation between tumbling period (T) and aspect ratio (P_D) is straight forward. Flow dichroism works well for small aspect ratio prolate or oblate nanoparticles. Similar results would be obtained when using a magnetic or electric field to control the particle dynamics which would also lead to a simple relation between P and the experimental observables. Moverover, rheo-optics is the only method which provides sample polydispersity.

Table 4: Aspect ratio of gold nanoparticles estimated from TEM and measured using DDLS and flow dichroism along with the polydispersity obtained from flow dichroism.

Sample	AR*	P_{TEM}	P_{DDLS}	P_D	σ_D
Au-nanorod-1	2.76 ± 0.5	2.3 ± 0.61	1.85 ± 0.65	1.7 ± 0.1	0.14 ± 0.03
Au-nanorod-2	3.43 ± 0.5	2.8 ± 0.64	1.35 ± 0.47	2.0 ± 0.1	0.05 ± 0.02
Au-nanorod-3	4.33 ± 0.6	3.4 ± 0.70	1.55 ± 0.54	NA	NA
Au-deca-1	0.62 ± 0.03	0.62 ± 0.04	NA	0.47 ± 0.03	0.17 ± 0.04
Au-deca-2	0.62 ± 0.025	0.63 ± 0.04	NA	0.55 ± 0.02	0.16 ± 0.03
Au-deca-3	0.62 ± 0.015	0.61 ± 0.03	NA	0.55 ± 0.01	0.05 ± 0.01

* Geometric aspect ratio

Conclusion

The aspect ratios of gold nanoparticles have been measured by three methods and the results compared. Transmission electron microscopy provides a geometric aspect ratio but good statistics can only be obtained with substantial effort. Optical methods on particles in suspension, such as DDLS and rheo-optics provided hydrodynamic aspect ratios. From DDLS correlation functions are simple to measure but the analysis to determine hydrodynamic aspect ratios is rather complex. Moreover, a small error in measuring diffusion coefficients results is a large error in calculated hydrodynamic aspect ratio. Rheo-optics provides a more robust result for small aspect ratio particles along with the associated polydispersity. The better results obtained from rheo-optical method is due to the use of a well defined flow field, which unlike Brownian motion can be applied in a precise and controlled way and due to the use of evolution of orientation angle. The latter is less affected by the effects of size and shape polydispersity compared to absolute quantities as scattering intensity and absorption. The orientation angle properly reflects the average of the distribution. We also showed that using dichroism even a complex shaped nanoparticles the effective hydrodynamic aspect ratio can be readily determined. The only draw back of rheo-optics is that the particles must be suspended in high viscosity fluid and their should be sufficient optical signal.

Acknowledgement

The authors thank Dr. Peter Holmqvist for useful discussion. We thank the EU for funding through the project NANODIRECT (Grant No. CP-FP 213948-2).

References

[1] Glotzer, S.C; Solomon, M.J. Anisotropy Of Building Blocks And Their Assembly Into Complex Structures. *Nat. Mat.* **2007**, 6, 557-562.

[2] Shipway, A. N.; Katz, E.; Willner, I. Nanoparticles Arrays on Surfaces for Electronic, Optical, and Sensor Applications. *ChemPhysChem* **2000**, 1, 18-52.

[3] Gangopadhyay, R.; De, A. Conducting Polymer Nanocomposites: A Brief Overview. *Chem. Mater.* **2000**, 12, 608-622.

[4] Hao, E.; Schatz, G. C.; Hupp, J. T. Synthesis and Optical Properties of Anisotropic Metal Nanoparticles. *J. Fluoresce.* **2004**, 14, 331-340.

[5] Perez-Juste, J.; Pastoriza-Santos, I.; Liz-Marzan, L. M.; Mulvaney, P. Gold Nanorods: Synthesis, Characterization and Applications. *Coord. Chem. Rev.* **2005**, 249, 1870-1901.

[6] Perez-Juste, J.; Rodriguez-Gonzlez, B.; Mulvaney, P. and Liz-Marzan, L. M. Optical Control and Patterning of Gold-Nanorod-Poly(vinyl alcohol) Nanocomposite Films. *Adv. Funct. Mater.* **2005**, 15, 1065-1071.

[7] Law, M; Sirbuly, D. J.; Johnson, J. C.; Goldberger, J.; Saykally, R. J.; Yang, P. Nanoribbon Waveguides for Subwavelength Photonics Integration. *Science* **2004**, 305, 1269-1273.

[8] Hadjipanayis, G. C. Nanophase hard magnets. *J. Magnet. Magnet. Mater.* **1999**, 200, 373-391.

[9] Elson, E. L. Cellular mechanics as an indicator of cytoskeletal structure and function. *Ann. Rev. Biophys. Biophys. Chem.* **1988**, 17, 397-430.

[10] Lin, Y.C.; Koenderink, G.H.; MacKintosh F.C.; and Weitz, D.A. Viscoelastic Properties of Microtubule Networks. *Macromolecules* **2007**, 40, 7714-7720.

[11] Jana, N.R. Shape effect in nanoparticle self-assembly. *Ange. Chemie Inter. Ed.* **2004**, 43, 1536-1540.

[12] Marek Grzelczak M., Vermant J., Furst E.M., Liz-Marzan L.M., Directed Self-Assembly of Nanoparticles *ACS Nano* **2010** 4, 3591-3605

[13] Onsager, L. The Effects of Shape on the Interaction of Colloidal Particles. *Ann. N.Y. Acad. Sci.* **1949**, 51, 627-659.

[14] Sader, J. E.; Pepperell, C. J.; Dunstan D. E. Measurement of the Optical Properties and Shape of Nanoparticles in Solution using Couette Flow. *ACS Nano* **2008**, 2, 334-340.

[15] Goldstein, J., Newbury, D.E., Joy, D.C., Lyman, C.E., Echlin, P., Lifshin, E., Sawyer, L., Michael, J.R., *Scanning Electron Microscopy and X-ray Microanalysis*; Springer, 2003.

[16] Russel W.B.; Saville D.A.; Schowalter W.R. *Colloidal Dispersions*; Cambridge University Press: Cambridge, 1989.

[17] Fuller G.G. *Optical Rheometry Of Complex Fluids*; Oxford University Press: Oxford, 1995.

[18] Wilcox C.D.; DoveS.B; McDavid W.D.; Greer D.B., UTHSCSA ImageTool, Department of Dental Diagnostic Science at The University of Texas Health Science Center, San Antonio, Texas **1996**.

[19] Berne, B. J.; Pecora, R. *Dynamic Light Scattering: With Applications to Chemistry, Biology, and Physics* ; Dover Publications 2000.

[20] Einstein, A. On the Movement of Small Particles Suspended in Stationary Liquid Required by the Molecular-Kinetic Theory of Heat. *Ann. Phys.* **1905**, 17, 549-560.

[21] Sutherland W. A dynamical theory of diffusion for non-electrolytes and the molecular mass of albumin. *Phil. Mag. S. 6, 9* **1905**, 54, 781-785.

[22] Rodriguez-Fernandez, J,; Perez-Juste, J,; Liz-Marzan, L. M.; and Lang P. R. Dynamic Light Scattering of Short Au Rods with Low Aspect Ratios. *J. Phys. Chem. C* **2007**, 111, 5020-5025.

[23] Droegemeier, J.; Eimer, W. Polarized and depolarized dynamic light scattering study on F-actin in solution: comparison with model calculations. *Macromolecules* **1994**, 27, 96Ð101.

[24] Lehner, D.; Lindner, H; Glatter, O. Determination of the Translational and Rotational Diffusion Coefficients of Rodlike Particles Using Depolarized Dynamic Light Scattering. *Langmuir* **2000**, 16, 1689Ð1695.

[25] Shetty, M.A.; Wilkins, G. M. H.; Nanda, J.; Solomon, M.J. Multiangle Depolarized Dynamic Light Scattering of Short Functionalized Single-Walled Carbon Nanotubes. *J. Phys. Chem. C* **2009**, 113, 7129-7133.

[26] Boersma, J. Viscous Force Constant for a Closed Cylinder. *J. Chem. Phys.* **1964**, 32, 1626-1632.

[27] Brenner, H. Rheology of a Dilute Suspension of Axisymmetric Brownian Particles. *Int. J. Multiph. Flow* **1974**, 1, 195-341.

[28] Ortega, A.; Garcia de la Torre, J. Hydrodynamic properties of rodlike and disklike particles in dilute solution. *J. Chem. Phys.* **2003** 119, 9914-9919

[29] Tanford, C. *The Hydrodynamic effect*, Wiley, 1973.

[30] Kekicheff, P.; Richetti P. Direct measurement of interactions in supermolecular fluids and liquid crystals. *Pure & Appl. Chem.* **1992**, 64, 1603-1609.

[31] Smith, J. N.; Meadows, J.; Williams, P. A. Adsorption of Polyvinylpyrrolidone onto Polystyrene Latices and the Effect on Colloid Stability. *Langmuir* **1996**, 12, 3773Ð3778

[32] Gonzalez A.L., Reyes-Esquada J.A., Noguez C. Optical properties of elongated noble metal nanoparticles *J. Phys. Chem. C* **2008** 112, 7356-7362.

[33] Ni W.; Zhou X.; Wang J. Tailoring Longitudinal Surface Plasmon Wavelengths, Scattering and Absorption of Gold Nanorods. *ACS Nano* **2008**, 2, 677-686.

[34] Jeffery G. B. The Motion Of Ellipsoidal Particles Immersed In A Viscous Fluid. *Proc. Roy Soc. Ser. A* **1922**, 102, 161-179.

[35] Meeten, G. H., Conservative Dichroism in the Rayleigh-Gans-Debye Approximation. *J. Colloid. Interface. Sci.* **1981** 84, 235-239

[36] Frattini, P. L.; Fuller, G. G. The Dynamics Of Dilute Colloidal Suspensions Subject To Time-Dependent Flow-Fields By Conservative Dichroism. *J. Colloid Interface Sci.* **1984**, 2, 506-518.

[37] Frattini, P. L.; Fuller, G. G. Conservative Dichroism Of A Sheared Suspension In The Rayleigh-Gans Light-Scattering Approximation. *J. Colloid Interface Sci.* **1987**, 119, 335-351.

[38] Johnson, S. J.; Fuller, G. G. The Optical Anisotropy of Sheared Hematite Suspensions. *J. Colloid Interface Sci.* **1988** 124, 441-451

[39] Breherton, F. P. The Motion Of Rigid Particles In A Shear Flow At Low Reynolds Number. *J. Fluid. Mech.* **1962**, 14, 284-304.

[40] Vermant, J.; Yang, H.; Fuller, G. G. Rheooptical Determination Of Aspect Ratio And Polydispersity Of Nonspherical Particles. *J. AIChE* **2001**, 47, 790-798.

[41] Nikoobakht, B.; El-Sayed, M. A. Preparation and Growth Mechanism of Gold Nanorods (NRs) Using Seed-Mediated Growth Method. *Chem. Mater.* **2003**, 15, 1957-1962.

[42] Liu, M.; Guyot-Sionnest, P. Mechanism of Silver(I)-Assisted Growth of Gold Nanorods and Bipyramids. *J. Phys. Chem. B* **2005**, 109, 22192-22200.

[43] Pastoriza-Santos, I.; Sanchez-Iglesias, A.; Garcia de Abajo, F. J.; Liz-Marzan, L. M. Environmental Optical Sensitivity of Gold Nanodecahedra. *Adv. Funct. Mater.* **2007**, 17, 1443-1450.

[44] Pellens, L.; Vermant, J.; Mewis, J. Deviations from the stress-optical relation in telechelic associative polymer solutions. *Macromolecules* **2005**, 38, 1911Ð1918.

Experimental

Synthesis of gold particles

Gold nanorods were prepared following the Ag+ assisted method proposed by Nikoobakht et al.[41] and modified by Liu et al.[42] . Briefly, first a gold seed solution was prepared by borohydride reduction of 5 mL 0.25 mM $HAuCl_4$ in an aqueous 0.1 M CTAB solution. For the synthesis of gold nanorods, 24 μL of seed solution was added to 10 mL of a growth solution containing 0.1 M CTAB, 0.5 mM $HAuCl_4$, 0.75 mM ascorbic acid, 0.12 mM silver nitrate and in the presence of 0.019M HCl, 0.01M HCl and in the absence of HCl, which resulted in gold rods with geometric aspect ratios (*AR*) of 2.7, 3.4 and 4.3 respectively.

A detailed procedure of gold decahedrons particle synthesis is give by Pastoriza-Santos et al.[43] . Briefly, 22 μM of an aqueous solution of 0.1136 M $HAuCl_4$(Aldrich) was added to 47.5 mL of a solution in a H_2O-DMF (Fluka) mixture (1:18; v/v) containing 0.017 g of PVP (Mw=40000, Fluka). Then, 2.5 mL of freshly prepared 10 mM $NaBH_4$ (Aldrich) solution was injected quickly into the solution under vigorous stirring. The gold sol was stirred for 2 hr at room temperature. A complete $NaBH_4$ decomposition was allowed to happen before using the gold seeds. Gold nanodecahedrons of dimensions 43, 100 and 173 nm were obtained.

TEM micrographs and the corresponding light extinction spectra for gold nanorods and gold decahedrons are shown in Figure 1. The scattering experiments were conducted at a wavelength of 647 nm for DDLS and 632.8 nm for dichroism.

DDLS

Time autocorrelation functions of the scattered intensity $g_2(q,t)$ were recorded with a standard DLS apparatus equipped with a Krypton (Kr) ion laser (λ_o = 647 nm, 100 mW). The scattering angle, θ, was varied from 40^o to 130^o in steps of 5^o covering a range of 8.835e-3 nm $<$ q $<$ 2.34e-2 nm, where $q = 4\pi n_s \sin(\theta/2)$ is the scattering vector. The polarization state of incident and scattered light was controlled with a $\lambda/2$ plate and a polarizer in the primary beam and an analyzer in the scattered beam (all polarizing optics are from Bernhard Halle Nachfl,Berlin; Germany). The scattered light was collected with a monomode optical fiber (OZ-Optics,Ottawa, Canada) and detected with a SO-SIPD dual photomultiplier unit by ALV Laserverstriebsgesellschaft mbH, Langen, Germany. The transistor-transistor logic (TTL) output of the avalanche diode was processed in the cross-correlation mode of a multiple tau correlator, ALV-5000. The shortest delay time, which is reliably accessible with this detector-correlator combination, is $\sim$100 ns. For each sample, a complete angular set of correlation functions was recorded in both vertical-vertical (VV) and vertical-horizontal (VH) modes.

Dichroism

Dichroism measurements have been performed using MCR300 controlled-stress rheometer (Paar Physica, Austria) as a mechanical platform and using an in-house developed optical train[44] . To monitor tumbling of anisotropic particles in the vorticity plane a Couette cell was used. The inner and outer radii of the Couette cell are 16.95 and 17.95 mm ($R_i/R_o = 0.94$) respectively and the height of the cylinder was 21 mm. Experiments were performed at room temperature. To reduce the effect of Brownian motion and to be in a high P*é*clet regime, gold nano particles were

suspended in 99.5 % glycerol (Sigma). The optical train consisted of He-Ne laser source (λ = 632.8nm, 10 mW), followed by a Glen-Thompson polarizer (P1, Newport, USA), a photoelastic modulator (PEM, Beaglehole Instruments, New Zealand) oriented at 45^o with respect to P1, a zero order quarter-wave plate (Newport) at 0^o with respect to P1. The beam is then passed into the Couette cell in the vorticity plane and the scattered light is collected by a photodiode. Data from the photodiode is sent through a low pass filter and the harmonic contents are passed to two lock-in amplifiers (Stanford Research Systems Model 530), which gives the first and the second harmonic (R_1 and R_2) as the output. The setup was calibrated in such a manner that the orientation in the flow direction corresponded to a positive dichroism. The concentration was chosen to be large enough to ensure a sufficient signal to noise ratio for the harmonic components R_1 and R_2, yet small enough to be in the single scattering limit and to remain in the hydrodynamically dilute regime. R_1 and R_2 along with calibration values for $J_1(A)$ and $J_2(A)$ are used to obtain the magnitude of the dichroism and the associated orientation angle.